Published OnlineFirst June 29, 2010; DOI: 10.1158/1535-7163.MCT-09-0768

Research Article

Molecular Cancer Therapeutics

Radiosensitization and Stromal Imaging Response Correlates for the HIF-1 Inhibitor PX-478 Given with or without Chemotherapy in Pancreatic Cancer

David L. Schwartz[1,2], James A. Bankson[3], Robert Lemos, Jr.[4], Stephen Y. Lai[5], Arun K. Thittai[1], Yi He[1], Galen Hostetter[6], Michael J. Demeure[6], Daniel D. Von Hoff[6], and Garth Powis[5]

Abstract

Growing tumors are hypoxic and respond to microenvironmental stress through increased expression of the hypoxia inducible factor-1α (HIF-1α) transcription factor, resulting in an adaptive switch to glycolytic metabolism, angiogenic signaling, survival, and metastasis. HIF-1α expression is associated with tumor resistance to cytotoxic therapy and inferior patient outcomes. Pancreatic cancer is the most hypoxic of all solid tumors and remains refractory to current chemoradiotherapy. We have seen nuclear HIF-1α in 88% of human pancreatic ductal carcinoma but in only 16% of normal pancreas. Stroma adjacent to the pancreatic ductal carcinoma also showed HIF-1α in 43% of cases. We investigated the novel selective HIF-1α inhibitor PX-478 on *in vitro* and *in vivo* radiation response of human pancreatic cancer models. Inhibition of HIF-1α by PX-478 increased cell killing by radiation. In mice with Panc-1, CF-PAC-1, or SU.86.86 pancreatic xenografts, concurrent administration of PX-478 potentiated the antitumor effects of fractionated radiation, with or without combined treatment with 5-fluorouracil or gemcitabine. Alternative sequencing of PX-478 with fractionated radiotherapy suggests optimal radiosensitization with concurrent or neoadjuvant administration of drug. Early tumor responses to combined PX-478/radiation treatment could be rapidly and repeatedly quantified by vascular imaging biomarkers. Dual-tracer dynamic contrast enhanced–magnetic resonance imaging and ultrasound imaging discriminated response to combined treatment prior to detection of differences in anatomic tumor size at 10 days posttreatment. Therefore, PX-478 is a mechanistically appealing and potentially clinically relevant enhancer of pancreatic cancer radiosensitivity, inhibiting tumor and stromal HIF-1 proangiogenic signaling and reducing the innate radiation resistance of hypoxic tumor cells. *Mol Cancer Ther; 9(7); 2057–67. ©2010 AACR.*

Introduction

Tumors, even micrometastases, have areas of hypoxia at the growing edge where growth outpaces new blood vessel formation (1). The abnormal architecture and blood flow dynamics of tumor vasculature, together with cycles of vasoconstriction and dilation, lead to periods of poor perfusion (2). More advanced tumors have additional areas of sustained hypoxia as blood vessels become compressed or obstructed by tumor cells (3). It has long been recognized that solid tumors with areas of hypoxia are the most aggressive and difficult tumors to treat (1). Hypoxic cancer cells are resistant to both chemotherapy and radiotherapy, and are a major reason for treatment failure (1, 3).

The most extensively studied tumor response to hypoxia is through hypoxia inducible factor-1α (HIF-1α), whose levels rapidly increase during hypoxia. HIF-1α is continuously expressed but degraded in normoxic conditions by the ubiquitin-proteasome system. O_2-dependent prolyl hydroxylases modify specific proline residues on HIF-1α, allowing binding of the von Hippel Lindau protein that recruits a ubiquitin-protein ligase complex containing elongin B, elongin C, and cullin, resulting in ubiquitination and degradation of HIF-1α by the 26S proteasome (4). Under hypoxic conditions O_2 is limiting for prolyl hydroxylation and HIF-1α is not degraded, allowing it to translocate to the nucleus where it binds with HIF-1β (also known as ARNT) to specific hypoxia response elements present in the promoter or enhancer regions of target genes (5). In addition to the inhibition of oxygen-dependent degradation, continued protein translation also contributes to the accumulation of HIF-1α in hypoxia when translation of most proteins is inhibited (6). The genes regulated by HIF-1α encode proteins involved in

Authors' Affiliations: Departments [1]Radiation Oncology, [2]Experimental Diagnostic Imaging, [3]Imaging Physics, and [4]Experimental Therapeutics, M.D. Anderson Cancer Center, Houston, Texas; [5]Head and Neck Surgery; and [6]TGEN, Phoenix, Arizona

Corresponding Author: Garth Powis, Department of Experimental Therapeutics, M.D. Anderson Cancer Center, 1400 Holcombe Boulevard, FC6.3044 Unit 422, Houston, TX 77030. Phone: 713-745-3366; Fax: 713-745-1710. E-mail: gpowis@mdanderson.org

doi: 10.1158/1535-7163.MCT-09-0768

Published OnlineFirst June 29, 2010; DOI: 10.1158/1535-7163.MCT-09-0768

erythropoiesis, glycolysis, promotion of cell survival, inhibition of apoptosis, and angiogenesis. Experimentally it has been shown that increased HIF-1 activity increases tumor growth, vascularization, and glucose metabolism, whereas loss of HIF-1 activity dramatically suppresses these responses. Not surprisingly it has been found that increased HIF-1α expression is a marker of aggressive clinical disease associated with poor patient prognosis and treatment failure in a number of cancers (7, 8).

Pancreatic cancer is an extremely lethal malignancy, with an overall 1-year survival rate of around 20% (9). Aggressive combinations of surgery, chemotherapy, and radiotherapy have yielded only incremental gains, and the benefit of adjuvant radiotherapy for resectable disease remains controversial (10). However, radiotherapy still has an important role to play in the treatment of pancreatic cancer, particularly locally advanced disease (11, 12). Pancreatic cancer is among the most hypoxic of all cancers (13) as a result of hypovascularity secondary to extensive desmoplasia (14, 15). HIF-1α protein levels are elevated in human primary pancreatic cancer whereas it is almost absent in normal pancreatic tissue (16, 17) Pancreatic cancer cell lines with constitutively expressed or transfected HIF-1α are resistant to chemotherapy and radiation-induced apoptosis, and display increased *in vivo* tumorigenicity (18). Inhibiting HIF-1α in pancreatic cancer is thus an attractive therapeutic strategy (19). PX-478 is an orally active selective inhibitor of HIF-1α translation (20), resulting in lowered levels of HIF-1α in cells and tumor xenografts (21), that is currently being tested in early clinical trials.

We investigated the combination of PX-478 and radiation, with or without cytotoxic chemotherapy, for treatment of pancreatic cancer xenografts, using dynamic contrast enhanced–magnetic resonance imaging (DCE-MRI) and high-frequency ultrasound vascular imaging (22–24) to study the downstream mechanistic effects of these treatments on tumor stromal vascular function.

Materials and Methods

Cells

BxPC-3, Panc-1, SU.86.86, CF-PAC-1, and MiaPaCa-2 pancreatic cancer cells were obtained from the American Tissue Type Culture Collection. MiaPaCa-2 cells were stably transfected with short hairpin RNA (shRNA) specific to HIF-1α (courtesy of Dr. Laura Gumbiner-Russo). The cells were grown in humidified 95% air, 5% CO_2 at 37°C in DMEM supplemented with 10% fetal bovine serum. All cell lines were tested to be mycoplasma free using a PCR enzyme-linked immunosorbent assay kit (Roche Diagnostics Inc.). Cell line lineage was confirmed by the M.D. Anderson Cancer Center Characterized Cell Line Core Service. PX-478 was synthesized by the M.D. Anderson Cancer Center Translational Chemistry Service.

Human pancreatic cancer immunohistochemistry

A tissue microarray (TMA) was constructed from 48 paraffin-embedded tumor blocks using an indexed manual tissue arrayer (Advanced EDM Automation). In addition, five cases of chronic pancreatitis were included as controls. When tissue was available, cases were triple punched with 1.0-mm core needles to include two tumor cores and one adjacent normal core. H&E-stained slides were reviewed by a pathologist, and desired regions were marked and transferred to the donor paraffin blocks.

The master TMA blocks were sectioned at 5 μm thickness, and water flotation was used for tissue section transfer. TMA slides were dewaxed, rehydrated, and subjected to heat-induced epitope retrieval using EDTA solution for 30 minutes using the BondMax autostainer (Leica Microsystems, Inc). Endogenous peroxidase was blocked and the slide was incubated for 30 minutes with HIf-1α antibody (25 ug/mL; BD Biosciences) and visualized by the Bond Polymer Refine Detection kit (Leica) using diaminobenzidine chromogen as substrate. Immunohistochemical staining localization was evaluated in adenocarcinoma and in peritumoral stroma separately. The vasculature was not included in the stromal component. Staining intensity was scored on a scale of 0 to 3, with a score of 3 indicating strong staining. If there was heterogeneous staining for either compartment for a given case, the higher intensity staining was scored.

Clonogenic survival assays

Panc-1 and BxPC-3 cells were grown to 70% confluence and incubated at 21% O_2 (normoxia) or 1% O_2 (hypoxia, via chamber) for 24 hours. Cells were treated with 25 μmol/L PX-478 for 24 hours and irradiated with a ^{137}Cs source (5.8 Gy/min), with atmospheric conditions maintained. Cells were assayed for colony formation by replating at specified numbers into 6-well plates in drug-free medium. The cells were immediately plated after irradiation, maintained for 12 days in normoxia, and stained with 0.5% crystal violet in absolute ethanol. Colonies with >50 cells were counted. Clonogenic survival curves were constructed from at least three independent experiments, and the radiation sensitizer enhancement ratio at 0.2 surviving fraction was calculated.

Western blotting

Western blotting for cellular HIF-1α was done as described previously (21).

In vivo antitumor studies

Approximately 10^7 BxPC-3, Panc-1, SU.86.86, or CF-PAC-1 pancreatic cancer cells in log cell growth were injected s.c. suspended in 0.2 mL PBS into the flanks of severe combined immunodeficient (SCID) mice. The animals were weighed weekly. Tumor diameters were measured twice weekly at right angles (d_{short} and d_{long}) with electronic calipers and were converted to volume

Published OnlineFirst June 29, 2010; DOI: 10.1158/1535-7163.MCT-09-0768

by the formula volume = $(d_{short})^2 \times (d_{long}) \div 2$. When the tumors reached volumes between 150 and 400 mm^3, the mice were stratified into groups of eight animals having approximately equal mean tumor volumes and PX-478, 5-fluorouracil (FU), or gemcitabine administration, and radiation commenced. Control animals received vehicle alone. When the tumor volume reached ≥1,500 mm^3 or became necrotic, the animals were euthanized. Log_{10} cell kill was calculated by the formula log_{10} cell kill = (tumor growth delay [day]) × (tumor doubling time [day] × 3.32). Tumor volume was measured as treated tumor volume/control tumor volume (T/C) % at the time of the last measurement before the control mice were euthanized. Tumor regression was measured as the maximum percent decrease in tumor volume relative to tumor volume at the start of treatment. The Mann-Whitney-Wilcoxon nonparametric test was used for assessing statistical significance ($P < 0.05$).

Animal irradiation and drug treatment

Irradiated tumors received 1 or 2 Gy via a ^{60}Co unit (1.8 Gy/min) with custom shielding daily for 5 consecutive days. Untreated control xenografts underwent mock irradiation. PX-478 was delivered via oral gavage at 4 to 30 mg/kg × 5 consecutive days. FU was administered i.v. at 20 mg/kg daily for 5 days, and gemcitabine at 120 mg/kg i.p. every 3 days for 3 doses.

Ultrasound imaging

Ultrasound imaging of xenografts was done with a Vevo 770 unit (VisualSonics), using a single-element transducer with 40 MHz center frequency. Power Doppler settings were held constant at 25dB Power Doppler gain, 5 KHz pulse repetition rate, 2.5 mm/s wall filter with 2 mm/s scan speed. Initial imaging of the tumor was done in B-mode to discriminate tumor boundaries, and Doppler images were acquired for a manually delineated region of interest encompassing the entire tumor. Relative vascular area was detected by color pixel density, defined as the ratio of the number of color pixels to total number of pixels within the region of interest.

MRI imaging

DCE-MRI was acquired using a 4.7T Biospec USR47/40 (Bruker Biospin MRI, Inc.). A high-throughput multianimal MRI configuration was used (25). Four linear volume resonators (35 mm ID) were arranged inside the 4.7T Biospec system with 40 cm bore and gradients with 26 cm ID, as previously described (26). A two-plane retinoic acid response element (RARE) imaging sequence and coronal T2-weighted RARE images (TE, 57 ms; TR, 2000 ms; FOV, 20 cm × 10 cm; matrix, 256 × 192; RARE factor 8) were used to verify animal positioning. Coronal T1-weighted scans (TE, 13.2 ms; TR, 1,000 ms; FOV, 6 cm × 3 cm; matrix, 256 × 128) were used for tumor localization. Axial T1-weighted spin-echo images (TE, 13.2 ms; TR, 1,000 ms; FOV, 3 cm × 3 cm; matrix, 256 × 56) and T2-weighted RARE images (TE, 80 ms; TR, 4,000 ms) with matched geometries were used for tumor visualization. Baseline T1 tissue levels were measured using a RARE saturation-recovery sequence (TE, 80 ms; TR, 350 ms to 4,000 ms; FOV, 3 cm × 3 cm; matrix, 128 × 128). Dual tracer DCE-MRI was acquired using large-molecular-weight (~228 kDa) PG-Gd-DTPA (27) and Magnevist (MW = 938 Da). A T1-weighted 3D fast, spoiled gradient echo sequence (TE, 2.7 ms; TR, 100 ms; 50° excitation angle; FOV, 3 cm × 3 cm; matrix, 128 × 96, 62 repetitions) was acquired repeatedly. After 1 minute of baseline scans, 0.2 mmol(Gd)/kg PG-Gd-DTPA was injected via tail vein catheter, and 5 minutes later, 0.2 mmol/kg Magnevist was injected. Signal intensity was normalized to the average value of muscle prior to administration of contrast. A semiautomated analysis of manually segmented dynamic data was done using Matlab. All biomarker measurements were normalized to the corresponding group average at baseline. The Mann-Whitney-Wilcoxon nonparametric test was used for assessing statistical significance ($P < 0.05$).

Results

PX-478 provides hypoxic radiosensitization *in vitro*

PX-478 has previously been shown to inhibit hypoxia-induced HIF-1α levels in Panc-1 and BxPC-3 pancreatic cancer cells with an IC_{50} between 10 and 25 μmol/L (21). Clonogenic survival assays showed radiosensitization of Panc-1 and BxPC-3 cells treated 24 hours prior to radiation with 25 μmol/L PX-478 in hypoxic conditions. For Panc-1 pancreatic cancer cells, the radiation sensitizer enhancement ratios (SER) at 0.2 surviving fraction were 1.42 and 1.05 in 1% and 21% O_2, respectively, as previously reported (28), and for BxPC-3 pancreatic cancer cells the ratios were 1.33 and 1.18. MiaPaCa-2 cells with HIF-1α knockdown (>90%) by shRNA provided SERs at 0.2 surviving fraction of 1.55 and 1.14 in 1% and 21% O_2%, respectively. Thus, both pharmacologic and genetic inhibition of HIF-1α in pancreatic cancer cells is associated with increased radiation tumor cell killing.

HIF-1α staining in human pancreatic cancer

HIF-1α staining was measured in 42 pancreatic ductal carcinoma (PDC) biopsy cores on a tissue microarray. Figure 1A shows typical stained sections with an acinar carcinoma for comparison. Cytokeratin staining was used as a reference. Figure 1B shows the scoring of HIF-1α staining on a scale of 0 to 3. Of 41 evaluable PDC sections, 36 (88%) showed HIF-1α staining (range, 0.5–3.0; median, 1.0) and only 5 sections had no staining. In comparison, only 5 of 31 (16%) evaluable normal pancreas showed HIF-1α staining. Of 32 sections with normal pancreas for comparison, PDC showed greater nuclear HIF-1α staining than normal pancreas in 24 of 32 (75%) cases. Stroma adjacent to the tumor also showed HIF-1α staining in 18 of 42 (43%) cases

Published OnlineFirst June 29, 2010; DOI: 10.1158/1535-7163.MCT-09-0768

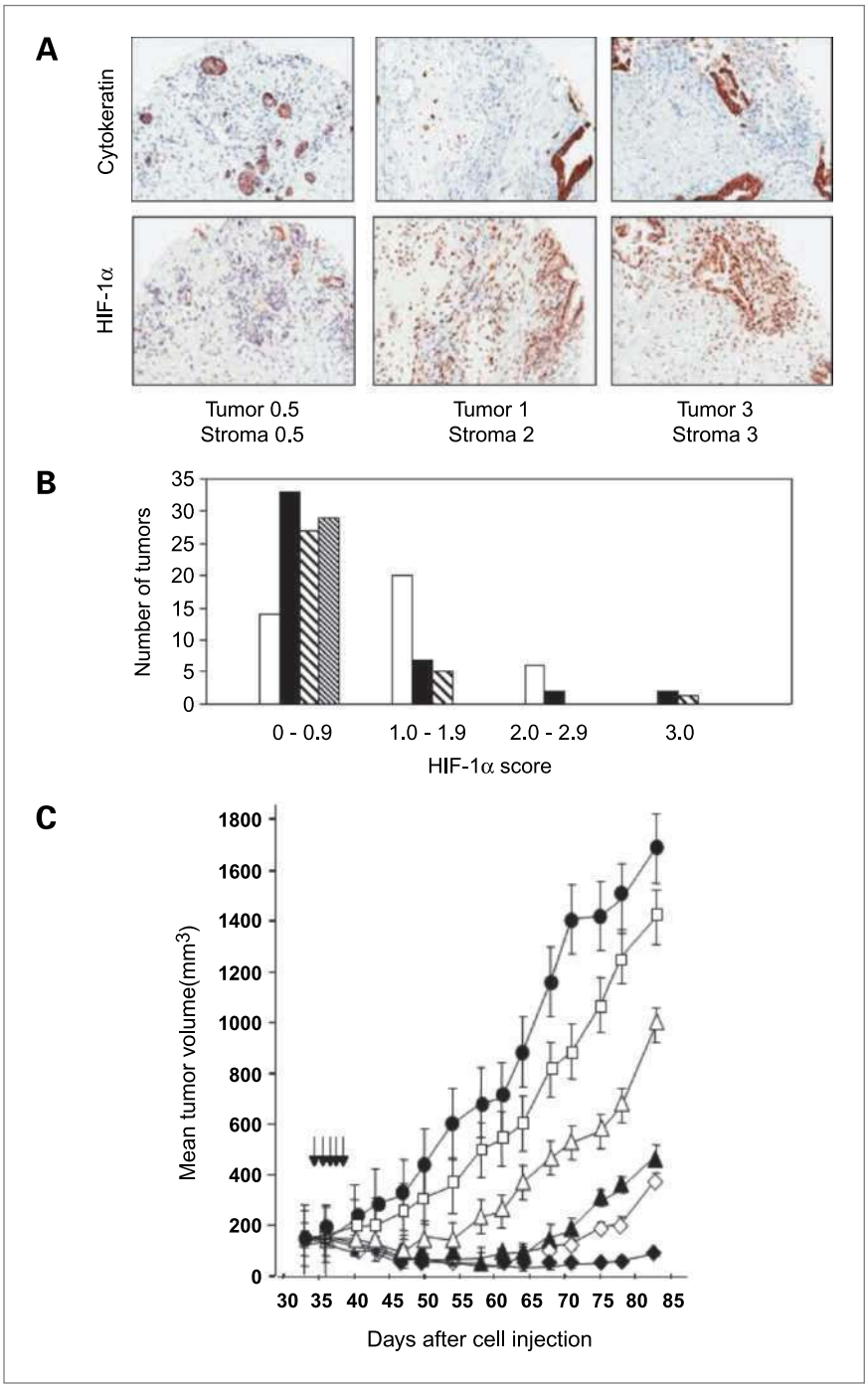

Figure 1. Immunohistochemistry of HIF-1 in patient tumors and PX-478 potentiation of the antitumor activity of fractionated radiation in Panc-1 tumor xenografts. A, typical staining of cytokeratin and HIF-1α. Left to right, two moderately well-differentiated ductal carcinomas and a moderately differentiated acinar carcinoma. The numbers are HIF-1α staining on a scale of 0 to 3 for the pancreatitis/tumor and for the adjacent stroma. B, histogram showing numbers of tumors in each staining range. Open bars, PDC (42 evaluable); filled bars, normal pancreas (42 evaluable); rough cross hatching, stroma adjacent to tumor (32 evaluable); fine cross hatching, stroma distant to tumor (30 evaluable). Stroma did not include blood vessel staining. C, female SCID mice with Panc-1 pancreatic tumor xenografts, 8 mice per group, were treated with vehicle alone (●);1 Gy radiation daily for 5 days (□); PX-478 10 mg/kg orally daily for 5 days (△); PX-478 20 mg/kg orally daily for 5 days (▲); PX-478 10 mg/kg orally daily for 5 days 1 hour before 1 Gy radiation daily for 5 days (◇); and PX-478 20 mg/kg orally daily for 5 days 1 hour before 1 Gy radiation daily for 5 days (♦). Arrows, daily dosing and/or radiation treatment. Values are the mean of 8 mice per group; bars, SE of mean.

(range, 0.5–3.0; median, 0.75; $P < 0.05$ compared with PDC), which was less than the PDC in 26 of 38 (68%) cases, the same in 11 of 38 (29%) cases, and greater than the PDC in 1 of 38 (3%) cases. In 18 of 32 (56%) cases HIF-1α staining was seen in the PDC in the absence of staining in the adjacent stroma. Stroma that was distant from the tumor showed HIF-1α staining in only one case.

PX-478 increases the antitumor activity of radiation

The antitumor activity of the HIF-1α inhibitor PX-478 and its effects on the response to radiation treatment were studied in Panc-1 pancreatic cancer xenografts (Fig. 1C). PX-478 given orally for 5 days caused a dose-dependent inhibition of tumor growth with T/C % at day 70 of the study (± SE, $n = 8$ mice per group) of 37.1 ± 5.3 and 13.7 ± 1.6 ($P < 0.01$ compared with

Published OnlineFirst June 29, 2010; DOI: 10.1158/1535-7163.MCT-09-0768

control) at 10 and 20 mg/kg PX-478, respectively, with 34.0% and 40.8% maximum tumor regression. Radiation at 1 Gy for 5 days alone had a small, nonsignificant effect on tumor growth with a T/C% of 62.8 ± 7.2 ($P > 0.05$) and no tumor regression. However, the concurrent daily combination of PX-478 and 1 Gy radiation for 5 days showed markedly increased antitumor activity with T/C% of 8.5 ± 2.1 and 2.5 ± 0.4 (both $P < 0.01$ compared with control) at 10 and 20 mg/kg, respectively, with 56.6% and 80.9% maximum tumor regression. At the end of the study (day 83), 4 of 8 mice treated with PX-478 20 mg/kg and 1Gy radiation had no macroscopically detectable tumor. Essentially similar results were obtained in a second study with PX-478 and radiation in Panc-1 pancreatic cancer xenografts (Table 1). Thus, concurrent administration of PX-478 for 5 days was able to markedly and dose-dependently potentiate the antitumor effects of fractionated radiation treatment, leading to tumor regression, prolonged growth delay, and in some animals, durable disease response at the end of the study.

PX-478 increases the antitumor activity of radiation and chemotherapy

The ability of PX-478 to potentiate the antitumor activity of radiation when used in combination with FU or gemcitabine chemotherapy, as used clinically in the treatment of pancreatic cancer and will be how PX-478

Table 1. Antitumor activity of PX-478 in combination with radiation and chemotherapy in pancreatic tumors

	Tumor size mm^3	Treatment	Dose mg/kg	Route schedule	Log cell kill	Regression %	T/C %
CF-PAC-1	200	PX-478	10	p.o. qd ×5	1.31	15.3	32.5*
		PX-478	20		3.87	38.2	10.8*
			Radiation 1 Gy qd ×5 and FU 20 mg/kg i.v. qd ×5†				
		Alone			0.45	0	65.3*
		PX-478	10	p.o. qd ×5	3.90	63.6	6.5*
		PX-478	20	p.o. qd ×5	Lethal		
SU.86.86	600	PX-478	4	p.o. qd ×5	0.56	0	32.1*
		PX-478	8		1.01	0	16.8*
			Radiation 1 Gy qd ×5 and FU 20 mg/kg i.v. qd ×5†				
		Alone			0.47	0	38.7*
		PX-478	4	p.o. qd ×5	1.21	0	16.1*
		PX-478	8	p.o. qd ×5	>1.65	66.7	3.0*
Panc-1	125	PX-478	5	p.o. qd ×5	3.30	0	54.0
		PX-478	10	p.o. qd ×5	3.47	0	36.7
		PX-478	20	p.o. qd ×5	5.20	72.0	9.8*
			Radiation 1 Gy qd ×5 and gemcitabine 120 mg/kg i.p. q3d ×3‡				
		Alone			0.52	0	35.8
		PX-478	5	p.o. qd ×5	4.16	35.6	13.0*
		PX-478	10	p.o. qd ×5	4.51	71.8	10.6*
		PX-478	20	p.o. qd ×5	6.94	79.0	7.6*
SU.86.86	400	PX-478	5	p.o. qd ×5	0.46	0	60.9
		PX-478	10	p.o. qd ×5	0.74	0	48.9*
		PX-478	20	p.o. qd ×5	1.11	11.7	28.7*
			Radiation 1 Gy qd ×5 and gemcitabine 120 mg/kg i.p. q3d ×3‡				
		Alone			1.84	24.6	24.5*
		PX-478	5	p.o. qd ×5	1.84	20.6	25.8*
		PX-478	10	p.o. qd ×5	2.45	40	19.6*
		PX-478	20	p.o. qd ×5	2.45	>75.8	15.8*

NOTE: Female SCID mice with s.c. pancreatic tumors with a mean tumor volume as shown at the start of treatment were administered radiation and chemotherapy with or without PX-478. Antitumor responses expressed as log cell kill, regression or test over control (T/C) were calculated compared with a vehicle-alone-treated control. There were 8 mice in each treatment group.
Abbreviations: p.o., orally; qd ×5, once a day for 5 days; q3d ×3, every 3 days for a total of 3 doses.
*$P < 0.01$ compared with control values (Mann-Whitney test).
†FU given 1 hour and PX-478 4 hours before radiation.
‡PX-478 given 4 hours before radiation and gemcitabine on days 12, 15, and 17.

Published OnlineFirst June 29, 2010; DOI: 10.1158/1535-7163.MCT-09-0768

is administered to patients, was examined (Table 1). PX-478 was toxic to mice when used concurrently with FU and radiation, requiring a 50% decrease in the maximum daily dose of PX-478 to 10 mg/kg or below. The dose limiting toxicity of PX-478 in mice is myelosuppression (20), so the combination of PX-478 with full dose FU which also causes myelosuppression may be the cause of increased toxicity. There was, however, a significant decrease in the T/C% when PX-478 was combined with FU and radiation at these lower doses of 3.0 ± 0.8 ($P < 0.01$ compared with control) at 8 mg/kg in SU.86.86 pancreatic cancer xenografts, and 6.5 ± 11.1 in CFPAC-1 pancreatic cancer xenografts ($P < 0.01$). Significant increases in $\log_{10}$ cell kill and % tumor regression were also seen with combined therapy. A different approach was adopted with gemcitabine, which also causes myelosuppresion, added to treatment with the radiation and PX-478. Radiation and PX-478 were given concurrently for 5 days, with gemcitabine then started 7 days later. Full-dose PX-478 at 20 mg/kg could be given with radiation and gemcitabine, in this way giving a T/C% of 7.6 ± 0.9 at 20 mg/kg in Panc-1 pancreatic cancer xenografts, and 15.8 ± 2.5 in SU.86.86 pancreatic cancer xenografts ($P < 0.01$ in both cases). The effect of PX-478 was dose dependent, and significantly increased $\log_{10}$ cell kill and % tumor regression were seen with combined treatment. Thus, PX-478 markedly potentiates the antitumor activity of fractionated radiation treatment and conventional cytotoxic chemotherapy in human pancreatic xenograft models.

In situ vascular imaging shows early biomarkers of tumor response to combined PX-478 and radiation

Figure 2 shows the treatment and imaging schedules for the different studies. Dual-tracer DCE-MRI was employed to measure vascular volume and vessel permeability in pancreatic tumors treated with a PX-478 and radiation (Fig. 3), with representative images shown in Fig. 4. There was a gradual attenuation of mean values of both imaging biomarkers in untreated tumors growing over two weeks. Reductions in these biomarkers mapped

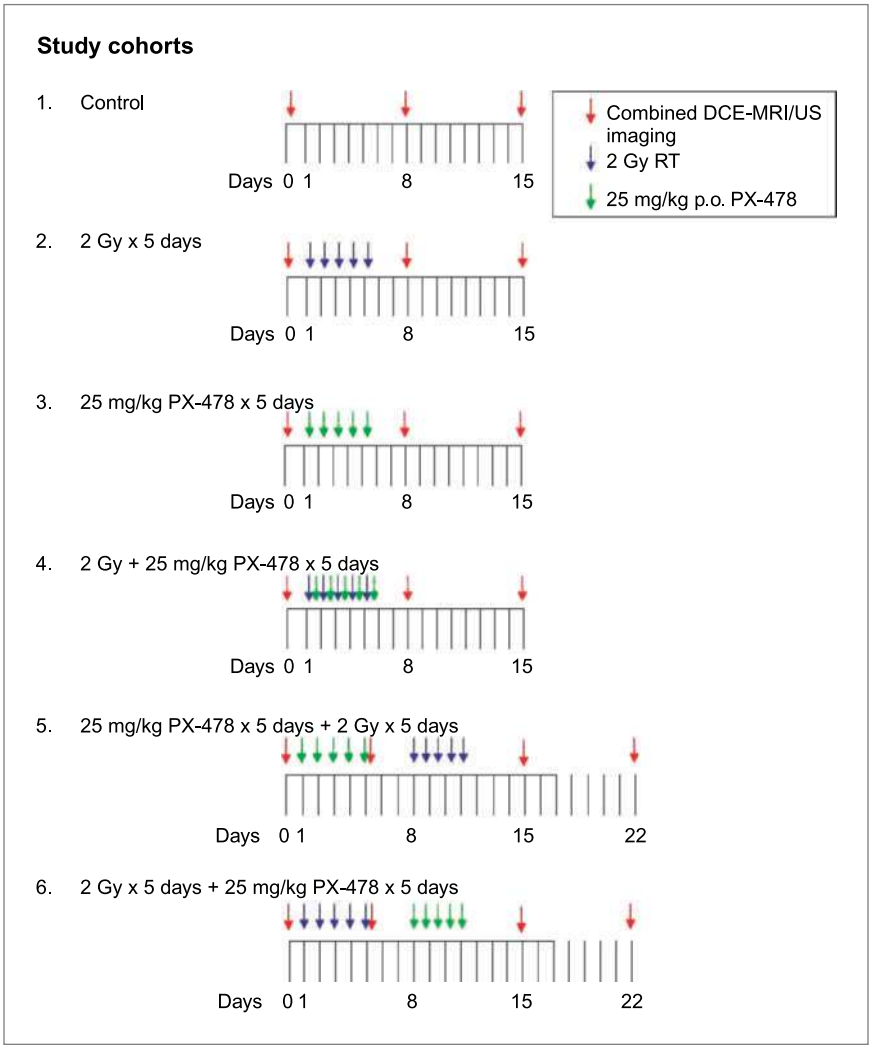

Figure 2. PX-478/radiation sequencing study treatment cohorts. Female SCID mice with Panc-1 pancreatic tumor xenografts, 8 mice per group, were treated with single-modality treatment or concurrent PX-478 25 mg/kg orally and 2 Gy radiation daily for 5 days per the indicated sequences. Timing of serial MRI and ultrasound measurements of each cohort is also indicated.

Published OnlineFirst June 29, 2010; DOI: 10.1158/1535-7163.MCT-09-0768

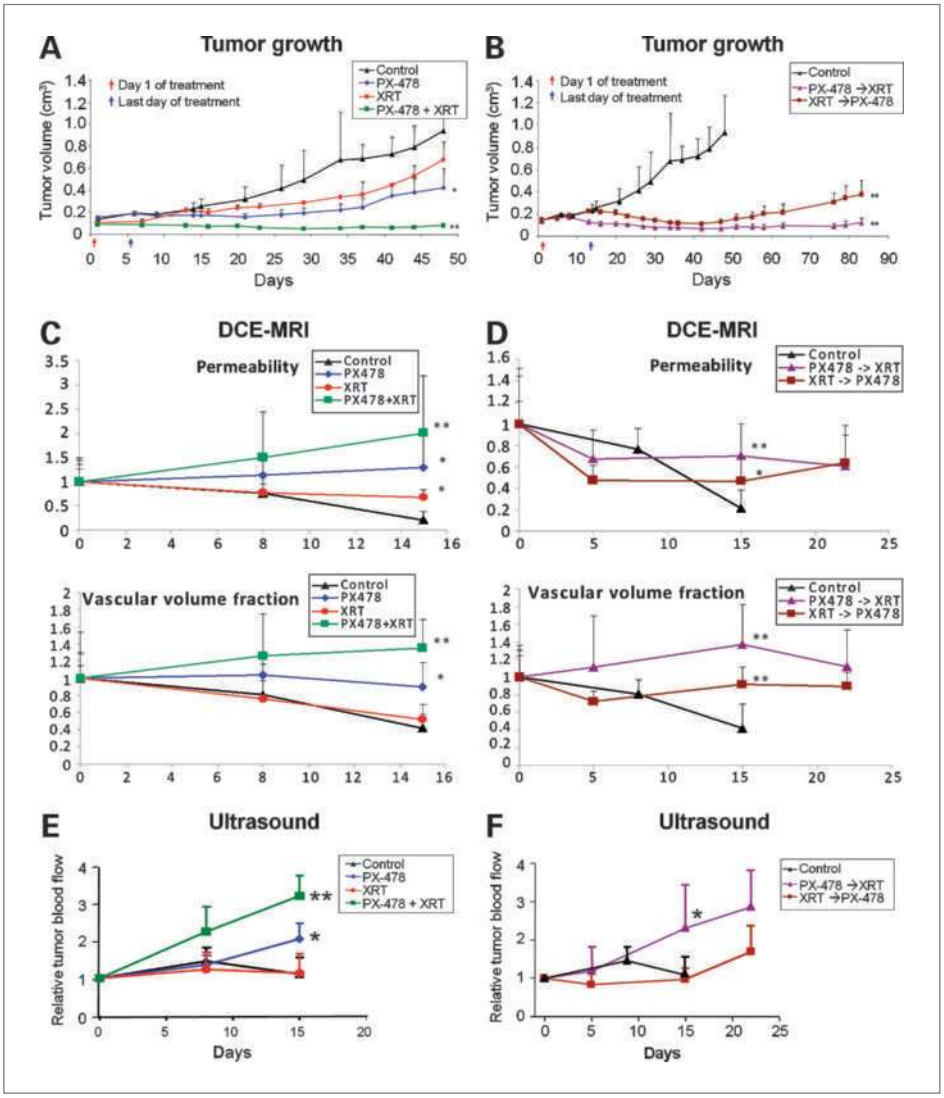

Figure 3. Tumor growth curves, DCE-MRI permeability/vascular volume fraction measurements, and power Doppler ultrasound measurements of tumor blood flow. Female SCID mice with Panc-1 pancreatic tumor xenografts, 8 mice per group, were treated with single-modality treatment or concurrent PX-478 25 mg/kg orally and 2 Gy radiation daily for 5 days (A, C, E), or over two weeks with sequenced PX-478 and radiation (XRT; B, D, F), as indicated. Statistical comparisons of results at each time point are with untreated controls, as reported as mean values ± SD; *, $P < 0.05$; **, $P < 0.01$.

in a generalized pattern throughout the central and peripheral regions of tumors, strongly suggestive of increasing interstitial pressure resulting in less efficient blood transport through the stromal microvasculature. Three days following treatment, no difference could be detected between control animals and those subjected to fractionated radiotherapy alone (Fig. 2, cohort 2). In contrast, single-agent PX-478 (Fig. 2, cohort 3) resulted in a trend by 3 days posttreatment (day 8) towards higher values of DCE-MRI–measured vascular permeability and vascular volume fraction (Fig. 3C and D and Fig. 4A and B). DCE-MRI vascular volume findings were corroborated by ultrasound tumor blood flow measurements (Fig. 3E). Both DCE-MRI and ultrasound biomarker changes were accelerated and intensified in tumors treated with concurrent PX-478 and fractionated radiation (Fig. 2, cohort 4). At 3 days posttreatment, vascular volume fraction (1.26 ± 0.49 versus 0.81 ± 0.17; $P = 0.051$) and ultrasound blood flow (2.2 ± 0.75 versus 1.2 ± 0.35; $P = 0.125$) were elevated relative to controls. Vascular integrity was compromised, as indicated by an increase in permeability (1.51 ± 0.94 and 0.76 ± 0.19; $P = 0.051$). All DCE-MRI and ultrasound vascular imaging parameters continued to increase relative to controls ($P < 0.01$) 10 days following concurrent PX-478 and radiation treatment (day 15) as these tumors regressed in size. Importantly, imaging biomarker measured differences between the control and combined treatment cohorts at 10 days posttreatment were found prior to detection of differential tumor growth between these groups ($P = 0.0079$ for imaging biomarkers; $P = 0.056$ for tumor size).

Serial DCE-MRI imaging of sequenced PX-478 and radiation treatment showed stable vascular volume fraction and permeability measurements over the 3-week imaging period (Fig. 3C and D). DCE-MRI

Published OnlineFirst June 29, 2010; DOI: 10.1158/1535-7163.MCT-09-0768

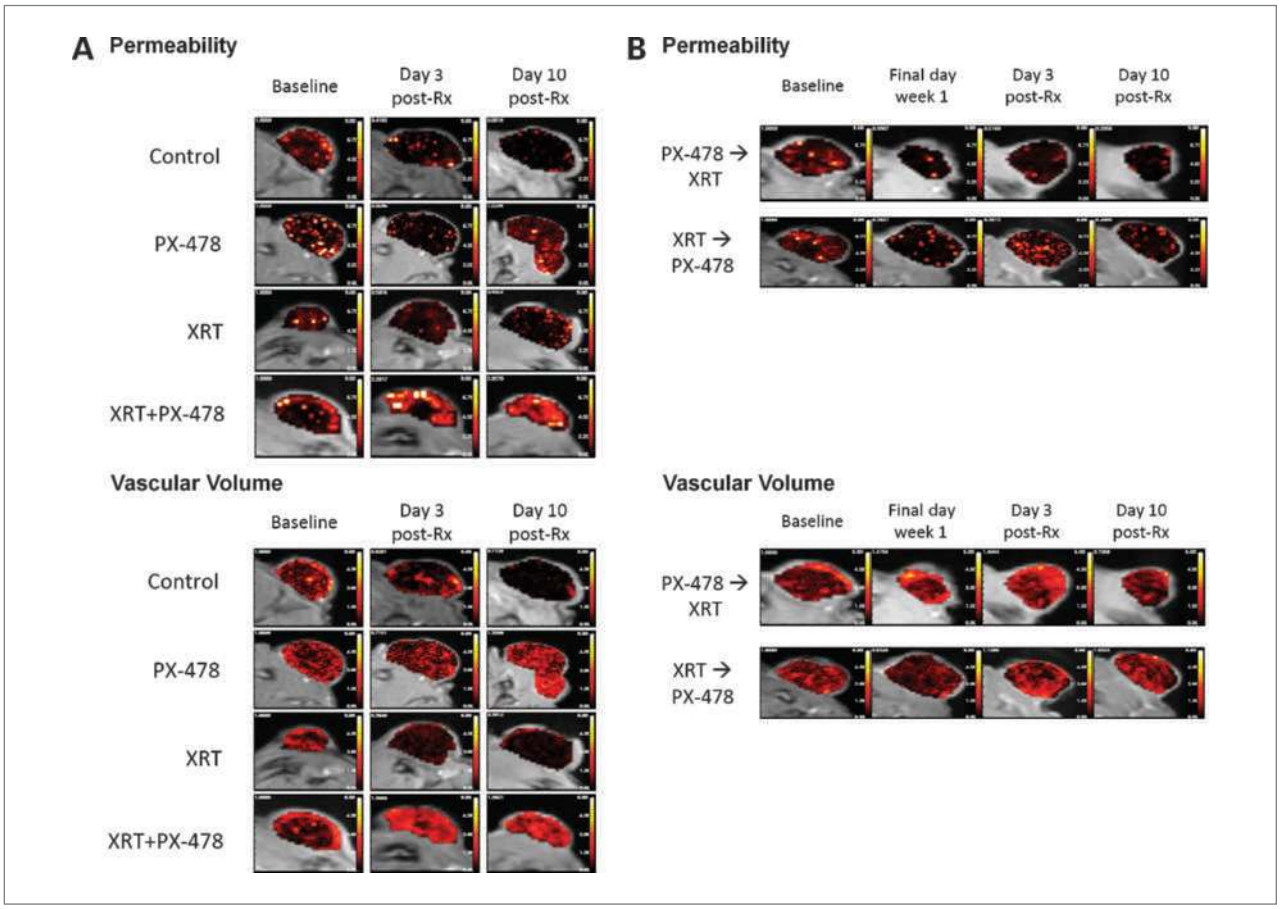

Figure 4. Representative serial DCE-MRI permeability/vascular volume fraction maps for indicated PX-478/radiation sequencing study treatment cohorts. Female SCID mice with Panc-1 pancreatic tumor xenografts were treated with single-modality treatment or concurrent PX-478 25 mg/kg orally and 2 Gy radiation daily for 5 days (A) or over two weeks with sequenced PX-478 and radiation (B).

vascular volume measurements 3 days posttreatment (day 15) were higher in tumors treated initially with PX-478 (Fig. 2, cohort 5) relative to decreasing values in controls ($P < 0.01$ for both permeability and vascular volume fraction). Differences between controls and animals treated initially with radiation (Fig. 2, cohort 6) were less striking ($P < 0.05$ for permeability; $P < 0.01$ for vascular volume fraction). Ultrasound measurements corroborated higher blood flow ($P < 0.05$) 3 days posttreatment in tumors treated first with PX-478 (2.3 ± 1.2 versus 1.0 ± 0.3 for controls), which continued to increase in treated tumors (2.8 ± 1.0) by 10 days following treatment. Increases in blood flow were delayed and less pronounced in the cohort first treated with radiation. Paralleling vascular imaging findings, a significant difference in relative tumor size change was detected 3 days (day 15) posttreatment between control animals and those treated with upfront PX-478 ($P = 0.008$), but not between control animals and those treated with radiation first. Despite these acute differential responses to treatment sequencing, all imaging biomarker outcome distinctions between the two cohorts were lost by 10 days posttreatment (day 22), indicating equivalent overall tumor response following completion of each respective 2-week treatment course. Consistent with these findings, both treatment sequences provided comparable, prolonged tumor growth delay outcomes.

Discussion

Pancreatic cancer remains refractory to aggressive chemotherapy and radiation therapy strategies, making the identification of novel biologic targets for this disease a priority (9). One such target is hypoxia. Pancreatic tumors are notorious for being poorly perfused (29) due to dense fibrotic inflammatory changes they induce in surrounding stromal tissues (14, 15). This has been recognized as a potential limiting factor in the delivery of systemic cytotoxic therapy and a possible mechanistic target for therapy (28).

We observed that a large proportion (88%) of human PDC expressed nuclear HIF-1α measured by immunohistochemistry whereas only 16% of normal pancreas

Published OnlineFirst June 29, 2010; DOI: 10.1158/1535-7163.MCT-09-0768

showed HIF-1α staining. Interestingly, stroma adjacent to the PDC also showed HIF-1α staining in 43% of cases, which was only slightly less than in the tumor. Stroma at a distance from the PDC showed no HIF-1α staining. It is likely that elevated HIF-1α levels in both PDC and adjacent stroma are a result of hypoperfusion and tumor hypoxia. In 56% of cases, however, HIF-1α staining was seen in the PDC without staining in the adjacent stroma, and this may be the result of constitutive elevation of HIF-1α, as has been reported for some PDC cell lines in normoxia (18).

HIF-1α is expressed at high levels in human pancreatic cancer models, and our previous work has shown these models to be susceptible to selective inhibition of HIF-1α with PX-478 (28). The HIF protein family serves as the physiologic cornerstone of cellular adaptation to microenvironmental stress. These proteins bind to specific DNA sequences in the promoters of a number of genes in conditions of low oxygen tension, stimulating cellular adaptation to microenvironmental stress through modulation of angiogenesis, glycolysis, apoptosis, differentiation, and proliferation (30, 31). Recent data suggest that radiotherapy induces loss of vascular integrity leading to tumor cell and stromal cell HIF-1–mediated proangiogenic signaling and downstream tumor vessel radioresistance (29, 32). Thus, selective inhibition of HIF-1 promises more effective enhancement of the effects of radiation than targeting of downstream angiogenic factors due to the more comprehensive direct and indirect vascular effects of HIF-1 blockade on tumor cells. This is particularly relevant to pancreatic cancer, given its known resistance to targeted antiangiogenic agents (33).

We observed that PX-478 causes a significant radiosensitization of pancreatic cancer cell lines in hypoxia (1% O_2) with a sensitizer enhancement ratio of 1.3 to 1.4, but also gives a small radiosensitization in normoxia (21% O_2) with a sensitizer enhancement ratio of 1.1 to 1.2. Genetic HIF-1α knockdown by shRNA yielded similar results in pancreatic cancer cells (over 1.5 in hypoxia and 1.1 in room air). HIF-1α protein is inappropriately expressed in aerobic conditions in the majority of pancreatic cancer cell lines examined (18), which provides a potential explanation for normoxic radiosensitization with targeted HIF-1α inhibition.

We examined the *in vivo* effects of the novel HIF-1 inhibitor PX-478 on response of human pancreatic tumor xenograft models to radiation treatment. Fractionated radiation at 1 or 2 Gy/day for 5 days provided nondurable tumor growth delay. Single-agent PX-478 administered orally over a 5-day period showed greater antitumor activity and tumor growth delay. However, combined treatment with both PX-478 and radiation was required for durable tumor control. There were relatively limited differences seen between neoadjuvant and adjuvant sequencing of PX-478 with fractionated radiation. Either sequencing schedule has potential mechanistic advantages. Neoadjuvant drug can reduce the hypoxic tumor fraction, yielding greater direct tumor cell response to radiation. Adjuvant drug can prevent HIF-1 dependent stromal adaptation to postradiation tumor ischemia. Thus, complementary combined early and adjuvant scheduling of PX-478 with radiation is worthy of testing. In this study, the modest improvements in acute response to neoadjuvant PX-478 relative to adjuvant PX-478 may simply be due to the fact that drug was given to smaller tumors in this cohort. Directly relevant to current clinical practice where FU or gemcitabine are used in combination with radiation, our data show that dose-modified PX-478 and radiation could be combined with FU or with delayed gemcitabine administration. Thus, PX-478 merits incorporation and testing with chemoradiation regimens which feature FU or gemcitabine.

DCE-MRI and ultrasound imaging permit serial evaluation of integrity and function of tumor stromal microvasculature and have the potential to provide quantifiable, predictive biomarkers of tumor response to vascular-targeted therapy (22, 24). We have previously employed DCE-MRI and ultrasound to mechanistically confirm that PX-478 sensitizes tumors to single-dose irradiation *in vivo* through inhibition of vascular recovery to radiation damage rather than direct tumor cell sensitization (29). We carried out these studies with single-agent, small-molecular weight tracer DCE-MRI. Our current series builds upon this experience through the novel use of dual (large and small molecular weight) tracer DCE-MRI (34) to permit discrimination of vascular blood volume from tumor vessel permeability. Ultrasound imaging suggested relatively stable blood flow in larger tumor vessels as untreated tumors continued to grow. However, dual-tracer DCE-MRI provided functional characterization of tumor microvessels, detecting a gradual reduction in both vascular volume fraction and permeability as these tumors continued to enlarge, consistent with inefficient blood delivery resulting from increasing tumor interstitial pressure. Fractionated radiation alone yielded no changes in tumor blood flow measures, which mirrored continued tumor growth. In contrast, single-agent PX-478 increased DCE-MRI and ultrasound vascular measures within one week following treatment, accompanied by a significant tumor growth delay. The combination of PX-478 and radiation, given either concurrently or sequentially, led to pronounced increases in DCE-MRI and ultrasound vascular measurements relative to controls, associated with marked inhibition of tumor growth.

Potential mechanisms of tumor stromal response and resistance to either fractionated radiation or PX-478 are distinct. Radiation directly damages tumor vessel integrity (35–38), leading to ischemic proangiogenic stromal adaptation and reperfusion of surviving tumor cells. PX-478 acts indirectly on vessels through blockade of tumor cell HIF-1–mediated paracrine proangiogenic signaling, yielding transient downstream vascular normalization (39) and improved matching of vascular supply to metabolic demand, ultimately leading to tumor cell repopulation. Given their complementary effects on tumor stromal vasculature, combined PX-478 and radiation has

Published OnlineFirst June 29, 2010; DOI: 10.1158/1535-7163.MCT-09-0768

appealing mechanistic promise, both with regard to therapeutic efficacy and potential utility of vascular imaging measures as response biomarkers and/or surrogate end points. Both we and others have shown that PX-478 (29) or genetic inhibition (40) of HIF-1α effectively radiosensitizes tumor cells through inhibition of supporting stromal vessels, particularly if timed to coincide with stromal adaptation events following radiation treatment. These earlier studies, however, used relatively large radiation doses at each administration (5–8 Gy), which would be expected to disturb endothelial viability and vascular integrity more significantly than the 2 Gy treatment fractions we tested in this study. Our *in vivo* results are consistent with PX-478 providing direct sensitization of hypoxic tumor cells to repeated lower-dose radiation treatments, akin to our *in vitro* results (Fig. 1B and C). Our imaging results support this mechanistically. Trends for universally increased vascular volume, flow, and permeability measurements following treatment, and the spatial homogeneity of these changes on DCE-MRI parameter maps (Fig. 4) are consistent not with drug-related vascular disruption as we have seen previously with large single-fraction radiation (29), but rather with decompressed tumor microvessel blood flow resulting from drug-related tumor cell depopulation and reduced interstitial pressure. Unlike tumors treated with large single-fraction radiation, recovery of tumor blood flow in this situation does not compensate for repeated direct tumor killing events resulting from daily administration of drug and radiation. From a clinical perspective, our current and previous results together suggest that PX-478 promises to provide strikingly versatile tumor sensitization across a spectrum of radiotherapy applications, including commonplace daily fractionated therapy as well as specialized single-fraction radiosurgical or intraoperative large dose treatments.

Our results also provide the important finding that DCE-MRI and ultrasound imaging promise the potential for early prediction of treatment response to clinically relevant combinations of PX-478 and radiation, and could accelerate detection of clinical outcomes beyond what is provided by standard tumor size–specific response criteria. We confirmed significant imaging biomarker measure differences 10 days posttreatment between the control and combined PX-478/radiation treatment cohorts which preceded detection of differences in anatomic tumor size changes. Because DCE-MRI and ultrasound vascular imaging are both routinely available in the clinical setting, validated predictive imaging biomarkers from these techniques could immediately impact efforts to streamline translation of targeted radiosensitization strategies with PX-478 or other vascular-targeting agents to appropriately selected patient populations.

In summary, we show that selective inhibition of HIF-1α by PX-478 inhibits the progression of otherwise radiorefractory human pancreatic cancer xenograft models following clinically relevant, daily fractionated radiation treatment. Concurrent administration of PX-478 with radiation, with or without combined treatment with FU or gemcitabine, provides durable regression of Panc-1, CFPAC-1, or SU.86.86 pancreatic xenografts which cannot be duplicated by any monotherapy approach. Clinically available DCE-MRI and ultrasound imaging techniques promise to significantly improve upon standard anatomic-based imaging response measures. Although fractionated radiotherapy does not significantly impact tumor vessel function in Panc-1 xenografts, PX-478 alone or in combination with radiation leads to acute tumor microvessel decompression and increased tumor blood flow. This does not compensate for direct tumor cell killing, and in fact can be capitalized upon as the basis for purposeful use of vascular imaging measures as novel, noninvasive response biomarkers. Continued experience with combined PX-478 and radiotherapy is validating this approach to be a mechanistically appealing strategy for sensitization of even the most refractory of tumor types, directly reducing the innate radiation resistance of hypoxic tumor cells and indirectly depriving all tumor cells of stromal vascular support through blockade of downstream angiogenic signaling.

Disclosure of Potential Conflicts of Interest

G. Powis owns stock in the Oncothyreon who own PX-478. No other potential conflicts of interest were disclosed.

Acknowledgments

We thank Dr. Laura Gumbiner-Russo for the HIF-1α shRNA knockdown MiaPaCa-2 cells and Cristina Palcu for determination of their radiation sensitivity.

Grant Support

CA109552, 095060, 017094, 095920, 016672 and 126577 from the National Cancer Institute.

The costs of publication of this article were defrayed in part by the payment of page charges. This article must therefore be hereby marked *advertisement* in accordance with 18 U.S.C. Section 1734 solely to indicate this fact.

Received 08/17/2009; revised 04/16/2010; accepted 05/05/2010; published OnlineFirst 06/29/2010.

References

1. Brown JM. Exploiting the hypoxic cancer cell: mechanisms and therapeutic strategies. Mol Med Today 2000;6:157–62.
2. Thomlinson R, Gray L. The histological structure of some human lung cancers and the possible implications for radiotherapy. Br J Cancer 1955;9:539–49.
3. Brown JM, Giaccia AJ. The unique physiology of solid tumors: opportunities and (problems) for cancer therapy. Cancer Res 1998; 58:1408–16.
4. Kaelin WG. Proline hydroxylation and gene expression. Ann Rev Biochem 2005;74:115–28.

Published OnlineFirst June 29, 2010; DOI: 10.1158/1535-7163.MCT-09-0768

5. Semenza GL. HIF-1 and tumor progession: pathophysiology and therapeutics. Trends Mol Med 2002;8:S62–7.
6. Koh MY, Spivak-Kroizman TR, Powis G. HIF-1 regulation: not so easy come, easy go. Trends Biochem Sci 2008;33:526–34.
7. Birner P, Schindl M, Obermair A, Breitenecker G, Oberhuber G. Expression of hypoxia-inducible factor-1αin epithelial ovarian tumors: its impact on prognosis and on response to chemotherapy. Clin Cancer Res 2001;7:1661–8.
8. Birner P, Schindl M, Obermair A, Plank C, Breitenecker G, Oberhuber G. Overexpression of hypoxia-inducible factor-1α is a marker for an unfavorable prognosis in early stage invasive cervical cancer. Cancer Res 2000;60:4693–6.
9. Pierantoni C, Pagliacci A, Scartozzi M, Berardi R, Bianconi M, Cascinu S. Pancreatic cancer: progress in cancer therapy. Crit Rev Oncol Hematol 2008;67:27–38.
10. Sultana A, Tudur Smith C, Cunningham D, et al. Systematic review, including meta-analyses, on the management of locally advanced pancreatic cancer using radiation/combined modality therapy. Br J Cancer 2007;96:1183–90.
11. Hazard L. The role of radiation therapy in pancreas cancer. Gastrointest Cancer Res 2009;3:20–8.
12. Loehrer PJ, Powell ME, Cardenes HR, et al. A randomized phase III study of gemcitabine in combination with radiation therapy versus gemcitabine alone in patients with localized, unresectable pancreatic cancer. J Clin Oncol 2008;26:4506, ASCO Annual Meeting.
13. Koong AC, Mehta VK, Le QT. Pancreatic tumors show high levels of hypoxia. Int J Radiat Oncol 2002;48:919–22.
14. Koito K, Namieno T, Nagakawa T, Morita K. Inflammatory pancreatic masses: differentiation from ductal carcinomas with contrast-enhanced sonography using carbon dioxide microbubbles. AJR Amer J Roentgenol 1997;169:1263–7.
15. Apte MV, Wilson JS. The desmoplastic reaction in pancreatic cancer: an increasingly recognized foe. Pancreatology 2007;7:378–9.
16. Zhong H, DeMarzo AM, Laughner E, et al. Overexpression of hypoxia-inducible factor 1α in common human cancers and their metastases. Cancer Res 1999;59:5830–5.
17. Buchler P, Reber HA, Buchler M, et al. Hypoxia-inducible factor 1 regulates vascular endothelial growth factor expression in human pancreatic cancer. Pancreas 2003;26:56–64.
18. Akakura N, Kobayashi M, Horiuchi I, et al. Constitutive expression of hypoxia-inducible factor-1α pancreatic cancer cells resistant to apoptosis induced by hypoxia and nutrient deprivation. Cancer Res 2001;61:6548–54.
19. Powis G, Kirkpatrick DL. Hypoxia inducible factor-1α as a cancer drug target. Mol Cancer Ther 2004;3:647–54.
20. Welsh S, Williams R, Kirkpatrick L, Paine-Murrieta G, Powis G. Antitumor activity and pharmacodynamic properties of PX-478, an inhibitor of hypoxia-inducible factor-1α. Mol Cancer Ther 2004;3:233–44.
21. Koh MY, Spivak-Kroizman T, Venturini S, et al. Molecular mechanisms for the activity of PX-478, an antitumor inhibitor of the hypoxia inducible factor-1 (alpha). Mol Cancer Ther 2008;7:90–100.
22. George ML, Dzik-Jurasz AS, Padhani AR, et al. Non-invasive methods of assessing angiogenesis and their value in predicting response to treatment in colorectal cancer. Br J Surg 2001;88:1628–36.
23. Cheung AM, Brown AS, Cucevic V, et al. Detecting vascular changes in tumour xenografts using micro-ultrasound and micro-ct following treatment with VEGFR-2 blocking antibodies. Ultrasound Med Biol 2007;33:1259–68.
24. Barrett T, Brechbiel M, Bernardo M, Choyke PL. MRI of tumor angiogenesis. J Magn Reson Imaging 2007;26:235–49.
25. Ramirez MS, Ragan DK, Kundra V, Bankson JA. Feasibility of multiple-mouse dynamic contrast-enhanced MRI. Magn Reson Med 2007;58:610–5.
26. Ramirez MS, Bankson JA. A practical method for 2D multiple-animal MRI. J Magn Reson Imaging 2007;26:1162–6.
27. Wen X, Jackson EF, Price RE, et al. Synthesis and characterization of poly(L-glutamic acid) gadolinium chelate: a new biodegradable MRI contrast agent. Bioconjugate Chem 2004;15:1408–15.
28. Schwartz DL, Powis G, Thitai-Kumar A, et al. The selective hypoxia inducible factor-1 inhibitor PX-478 provides in vivo radiosensitization through tumor stromal effects. Mol Cancer Ther 2009;8:947–58.
29. Von Hoff DD, Korn R, Mousses S. Pancreatic cancer–could it be that simple? A different context of vulnerability. Cancer Cell 2009;16:7–8.
30. Semenza GL. HIF-1: mediator of physiological and pathophysiological responses to hypoxia. J Appl Physiol 2000;88:1474–80.
31. Harris AL. Hypoxia–a key regulatory factor in tumour growth. Nat Rev Cancer 2002;2:38–47.
32. Moeller BJ, Cao Y, Li CY, Dewhirst MW. Radiation activates HIF-1 to regulate vascular radiosensitivity in tumors: role of reoxygenation, free radicals, and stress granules. Cancer Cell 2004;5:429–41.
33. Van Cutsem E, Vervenne WL, Bennouna J, et al. Phase III trial of bevacizumab in combination with gemcitabine and erlotinib in patients with metastatic pancreatic cancer. J Clin Oncol 2009;27:2231–7.
34. Orth RC, Bankson J, Price R, Jackson EF. Comparison of single- and dual-tracer pharmacokinetic modeling of dynamic contrast-enhanced MRI data using low, medium, and high molecular weight contrast agents. Magn Reson Med 2007;58:705–16.
35. Garcia-Barros M, Paris F, Cordon-Cardo C, et al. Tumor response to radiotherapy regulated by endothelial cell apoptosis. Science 2003;300:1155–9.
36. Paris F, Fuks Z, Kang A, et al. Endothelial apoptosis as the primary lesion initiating intestinal radiation damage in mice. Science 2001;293:293–7.
37. Guelinckx PJ, Boeckx WD, Fossion E, Gruwez JA. Scanning electron microscopy of irradiated recipient blood vessels in head and neck free flaps. Plast Reconstr Surg 1984;74:217–26.
38. Ceelen W, Smeets P, Backes W, et al. Noninvasive monitoring of radiotherapy-induced microvascular changes using dynamic contrast enhanced magnetic resonance imaging (DCE-MRI) in a colorectal tumor model. Int J Radiat Oncol Biol Phys 2006;64:1188–96.
39. Jain RK. Normalization of tumor vasculature: an emerging concept in antiangiogenic therapy. Science 2005;307:58–62.
40. Moeller BJ, Dreher MR, Rabbani ZN, et al. Pleiotropic effects of HIF-1 blockade on tumor radiosensitivity. Cancer Cell 2005;8:99–110.

AACR American Association for Cancer Research

Molecular Cancer Therapeutics

Radiosensitization and Stromal Imaging Response Correlates for the HIF-1 Inhibitor PX-478 Given with or without Chemotherapy in Pancreatic Cancer

David L. Schwartz, James A. Bankson, Robert Lemos, Jr., et al.

Mol Cancer Ther 2010;9:2057-2067. Published OnlineFirst June 29, 2010.